High-Performance Non-Fused Electron Acceptor with Precisely Controlled Side Chain Fluorination

Kexin Yu[†,‡], Tao Zhou[#], Wenting Liang[†], Xiaoli Zhou[†], Xiaopeng Xu[#,*], Liyang Yu[#], Bo Hou[⊥], Yangen Huang[‡], Fengkun Chen[†,§,*], Yaozu Liao[†,*], Huawei Hu[†,Δ,*]

[†] State Key Laboratory for Modification of Chemical Fibers and Polymer Materials, College of Materials Science and Engineering, Donghua University, Shanghai 201620, China

E-mail: huaweihu@dhu.edu.cn; yzliao@dhu.edu.cn; fkchen@dhu.edu.cn

[‡] College of Chemistry and Chemical Engineering, Donghua University, Shanghai 201620, China

[⊥]School of Physics and Astronomy, Cardiff University, Cardiff CF243AA, U.K.

[§]Shanxi-Zheda Institute of Advanced Materials and Chemical Engineering

[#] College of Chemistry and School of Chemical Engineering, Sichuan University, Chengdu 610065, China

E-mail: xpxu@scu.edu.cn

[Δ]Key Lab of Fluorine and Silicon for Energy Materials and Chemistry of Ministry of Education/National Engineering Research Center for Carbohydrate Synthesis, Jiangxi Normal University, 99 Ziyang Avenue, Nanchang 330022.

Abstract:

Modification of the molecular packing of non-fullerene acceptors through fluorination represents one of the most promising strategies to achieve highly efficient organic solar cells (OSCs). In this work, three non-fused electron acceptors, namely DTCBT-Fx (x = 0, 5, 9), with precisely controlled amounts of fluorine atoms in the side chains are designed and synthesized, and the effect of side chain fluorination is systematically

studied. The results demonstrate that the light absorption, energy levels, as well as molecular ordering, and film morphology could be effectively tuned through precisely controlling the side chain fluorination. DTCBT-F5 with appropriate fluorine functionalization exhibits suitable miscibility with the donor polymer (PM6), leading to diminished charge recombination and improved charge carrier mobility. Consequently, a promising power conversion efficiency of 12.7% was obtained for DTCBT-F5-based solar cells, which outperforms those OSCs based on DTCBT-F0 (11.4%) and DTCBT-F9 (11.6%), respectively. This work demonstrates that precise control of the fluorine functionalization in side chains of non-fused electron acceptors is an effective strategy for realizing highly efficient OSCs.

Key Words: organic solar cells, non-fused electron acceptors, fluorination, miscibility, molecular ordering

1. Introduction

Organic solar cells (OSCs) have been extensively investigated owing to their promising application prospects in producing large-area, semitransparent, and mechanical flexible modules through utilizing low-cost fabrication techniques.[1-5] Over the past few years, great efforts have been made to boost the power conversion efficiency (PCE) of OSCs, and one breakthrough in this field is the transfer from traditional fullerene electron acceptors to non-fullerene small molecular acceptors (SMAs).[6-8] Novel fused ring non-fullerene SMAs, including A-D-A-type (ITIC) and A-DA'D-A-type (Y6) materials which typically consist of two electron-deficient ending groups as well as a large fused core with bulky side chains, have boosted the PCE beyond 18% for single junction, and 20% for tandem OSCs, respectively.[9-13] The high performance of these OSCs is highly dependent on the broad light absorption and enhanced charge carrier mobilities of fused ring non-fullerene SMAs owing to their outstanding coplanarity.[14-15] Nevertheless, the synthesis of fused SMAs typically comprises labor-intensive and time-consuming ring-closure reactions, which could potentially raise the commercial application cost of OSCs.[16-17] Consequently, the design and synthesis of high-performance SMAs with

straightforward synthetic routes represent a promising strategy to realize robust and low-cost OSCs.[18-20]

The device performance of OSCs is highly dependent on the microstructure morphology of the active layer which can be finely tuned by the molecular structure and miscibility.[21-23] Typically, the molecular properties of SMAs can be rationally designed and feasibly tuned by modifying the π-conjugated central unit as well as the electron-withdrawing end groups. For example, changing the backbone constituent from thiophene units to selenium moieties,[24] tuning the size of π-conjugated core,[25] introducing electron-withdrawing or electron-donating groups (i.e., through fluorination,[26-27] chlorination,[28-29] methoxylation,[30] and methylation[31]), and π-extending the ending 1,1-dicyanomethylene-3-indanone groups[32] have been extensively reported to tune the macroscopic properties of non-fullerene SMAs. In addition, proper side chains are also critical because they have a great influence on the absorption, energy levels, solution processibility, molecular packing, as well as intermolecular interactions, which all play substantial roles in manipulating the device efficiency of OSCs.[33-37]

Fluorination is widely used to manipulate the chemical and physical properties of organic molecules due to the high electronegativity nature of the fluorine atoms.[38] The incorporation of fluorine atoms into the backbone or the side chains of organic molecules has been shown to effectively tune the energy levels, molecular packing, surface energy, as well as thin film morphology of organic semiconductors used in the field of OSCs and organic thin film transistors.[39-41] For example, trifluoromethyl groups have been successfully introduced into ending groups of both ITIC-type and Y6-type non-fullerene SMAs to adjust the energy levels, molecular interaction, and charge transport proprieties.[42-43] More recently, fluorinated alkyl chains have been implanted in the pyrrole unit within the Y-series non-fullerene SMAs to decrease the surface energy which could effectively regulate the vertical phase distribution of the bulk-heterojunction layer, thus leading to high-performance OSCs.[44] However, the structure-property-performance relationship of alkyl chain fluorination still remains unclear. Moreover, to the best of our knowledge, the incorporation of a fluorinated alkyl side

chain in non-fused SMAs, and thus their effects on the device performance, is unexplored.

In this work, for the first time, we reported the influence of multi-fluorinated side chains on the molecular ordering and device performance of non-fused SMAs. Three pairs of asymmetric non-fused SMAs, namely DTCBT-Fx (x = 0, 5, 9), with precisely controlled fluorine functionating in the side chains are designed and synthesized. The asymmetric structure was employed based on the following considerations: first, the S···O and C-H···O intramolecular noncovalent interaction ensures a C-shaped molecular, which is demonstrated to be favorable molecular shape for high performance non-fused SMAs;[45-47] second, it enables us to have more precise control over the fluorine content in the materials. The chemical structures of these non-fused electron acceptors are shown in Figure 1a. The influence of the number of fluorine atoms in the side chain was systematically investigated, and the results exhibited that the light absorption, energy levels, as well as the molecular ordering, and bulk-heterojunction morphology could be finely modified through side chain fluorination. When pairing with the wide bandgap donor polymer PM6 (Figure S1), the DTCBT-F5-based blend film shows appropriate miscibility, diminished charge recombination, and improved charge carrier mobility. Consequently, the DTCBT-F5-based devices obtained an enhanced short-circuit current density (J_{SC}) and fill factor (FF), and thus the best PCE of 12.7%, which outperforms those devices based on DTCBT-F0 (11.4%) and DTCBT-F9 (11.6%), respectively. This work demonstrates that precise control of the fluorine functionalization in side chains of non-fused SMAs represents a potent approach for obtaining high J_{SC} and FF towards highly efficient OSCs.

2. Results and Discussion

2.1. Materials Synthesis and Characterization. The synthetic routes of DTCBT-F0, DTCBT-F5, and DTCBT-F9 are illustrated in Scheme S1, and the detailed information are described in the Supporting Information. The aldehyde intermediates (M1-3) are obtained by direct arylation coupling reaction of 1,4-dibromo-2,5-bis((2-ethylhexyl)oxy)benzene with DTC-CHO, T-Fx-CHO.[48] Subsequently, DTCBT-Fx (x =

0, 5, 9) are synthesized in yields of 62, 61, and 60% by the Knoevenagel condensation reaction of M1-3 with 2-(5,6-dichloro-3-oxo-2,3-dihydro-1H-inden-1-ylidene)malononitrile (2Cl-IC) in chloroform. The resulted non-fused acceptors are fully characterized by nuclear magnetic resonance spectroscopy and mass spectrometry (see the Supporting Information). DTCBT-Fx (x = 0, 5, 9) all exhibit good solubility in commonly used organic solvents such as dichloromethane, chloroform, and toluene at room temperature, indicating their suitability for solution-based fabrication of OSCs. An investigation of the thermal stability of DTCBT-F0, DTCBT-F5, and DTCBT-F9 was carried out using a thermogravimetric analysis. As shown in Figure S2 and Table S1, the decomposition temperatures (T_d, 5% weight loss) of DTCBT-F0, DTCBT-F5, and DTCBT-F9 were measured to be 308.9, 329.3, and 326.7 °C, respectively. This enables them with good thermal stability, rendering them suitable for prolonged device operation.

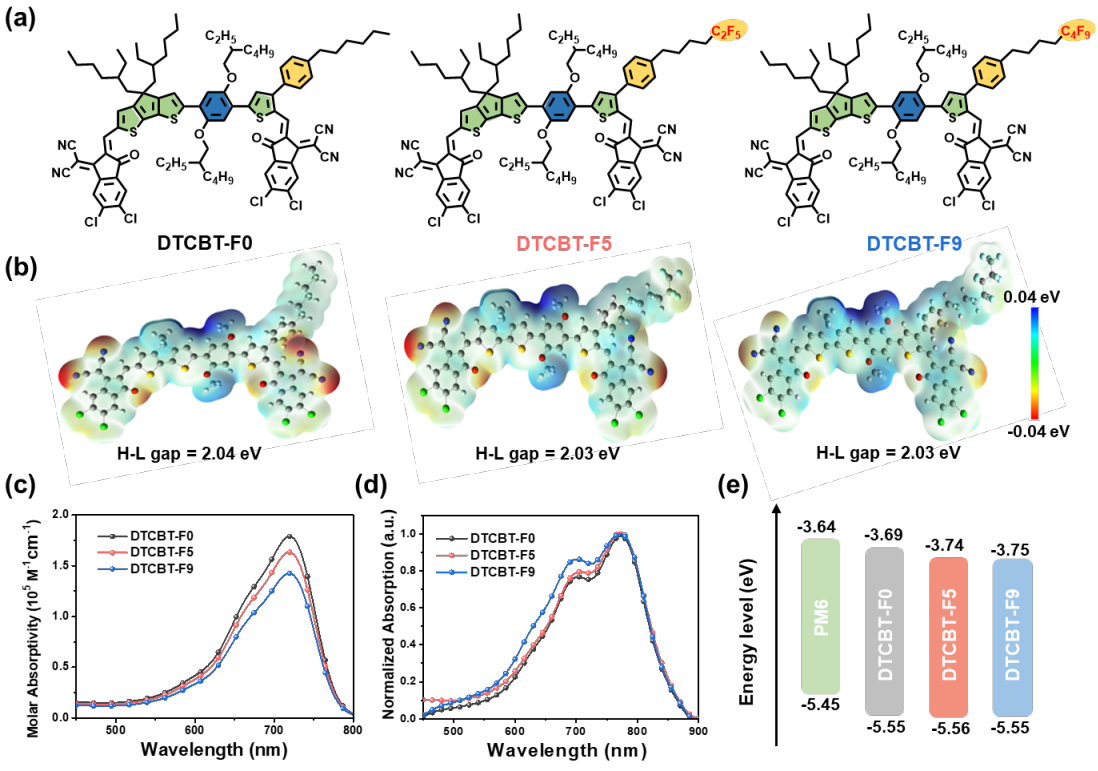

Figure 1. (a) Chemical structures of DTCBT-F0, DTCBT-F5, and DTCBT-F9; (b) Electrostatic potentials of DTCBT-F0, DTCBT-F5, and DTCBT-F9; (c) Absorption spectra of DTCBT-F0, DTCBT-F5, and DTCBT-F9 in chloroform solution; (d) Normalized absorption spectra of DTCBT-F0, DTCBT-F5, and DTCBT-F9 in neat

films; (e) Energy-level diagram of PM6, DTCBT-F0, DTCBT-F5, and DTCBT-F9.

2.2. Optical and Electronic Properties. In Figure 1c and Figure 1d, the UV-Vis absorption spectra of DTCBT-F0, DTCBT-F5, and DTCBT-F9 are shown in both chloroform solution and film. In view of the identical backbone of three SMAs, the solution absorption spectra in the range of 450-800 nm are approximately the same with a similar maximum absorption peak at 719 nm. The molar extinction coefficients (ε) are 1.79×10^5, 1.63×10^5, and 1.43×10^5 M^{-1} cm^{-1}, for DTCBT-F0, DTCBT-F5, and DTCBT-F9, respectively. As the absorption maximum position moves to 771 nm, the absorption spectrum shows a red-shift in the solid state. The absorption onsets for DTCBT-F0, DTCBT-F5, and DTCBT-F9 are determined at 866 nm, 868 nm, and 867 nm, suggesting their similar optical bandgap (E_g^{opt}) of 1.43 eV. In addition, the 0–0/0–1 peak intensity ratio of the three SMAs indicate the formation of *J*-aggregation in thin films with slightly different aggregation characteristics,[49] with DTCBT-F9 having the lowest intensity ratio of 0–0/0–1 peak.

The electrochemical properties investigated by the cyclic voltammetry are illustrated in Figure S3. According to the CV curves, the highest occupied molecular orbital (HOMO) and the lowest unoccupied molecular orbital (LUMO) are found to be –5.55/–3.69 eV –5.56/–3.74 eV, and –5.55/–3.75 eV for DTCBT-F0, DTCBT-F5 and DTCBT-F9, respectively. A further calculation shows that the electrochemical bandgaps (E_g^{ele}) were 1.86, 1.82, and 1.80 eV, respectively. The electrochemical band gap are generally slightly larger than the optical band gaps, which is consistent with the previous report.[50] The result suggests that the introduction of fluorine atoms into side chains could lower the LUMO energy levels. As a result, it is anticipated that a decreased open circuit voltage (V_{OC}) would be obtained for the fluorinated materials-based devices, due to their smaller energy disparity between the HOMO level of the donor and the LUMO level of the acceptor.

Molecular conformations, electronic cloud distributions, and molecular surface

electrostatic potentials (ESP) were calculated using density functional theory (DFT). As illustrated in Figure 1b, positive electrostatic potentials are mainly localized on the molecular backbone while negative electrostatic potentials are present on the electron-withdrawing end groups, resulting in an intermolecular electric field in interactions with the PM6, beneficial for efficient charge generation. With fluorine atoms in side chains, the torsion angle of DTCBT-F5 is smaller (Figure S4), which promotes coplanarity, facilitates charge carrier transport and improves molecular packing. Furthermore, the LUMOs are delocalized throughout the conjugate backbone while HOMOs are mainly located at the electron-donating part, and this distribution promotes the effective transfer of electrons and holes. The HOMO/LUMO energy levels for the three SMAs correspond to the previously described trend of narrowing band gaps, with -5.52/-3.48 eV, -5.56/-3.53 eV and -5.56/-3.53 eV, respectively.

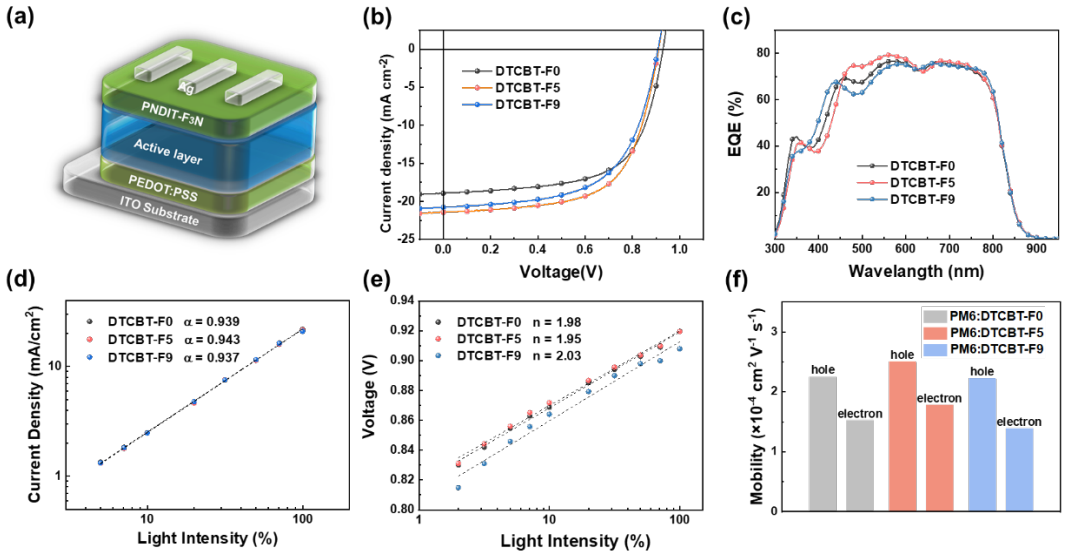

Figure 2. (a) Schematic diagram of device structure in this work; (b) Current density-voltage (*J-V*) curves of OSCs based on PM6:DTCBT-F0, PM6:DTCBT-F5, and PM6:DTCBT-F9; (c) EQE spectra of corresponding devices; (d) J_{SC} versus light intensity of the optimized devices based on DTCBT-F0, DTCBT-F5, and DTCBT-F9; (e) V_{OC} versus light intensity of the optimized devices based on DTCBT-F0, DTCBT-F5, and DTCBT-F9; (f) The hole and electron mobilities of the OSCs based on DTCBT-F0, DTCBT-F5, and DTCBT-F9.

2.3. Photovoltaic Performances. In order to investigate the effect of different amounts of fluorine atoms in the side chains of non-fused SMAs on their performance of OSCs, we fabricated OSCs with ITO/PEDOT:PSS/PM6:SMA/PNDIT-F3N/Ag conventional configurations, as shown in Figure 2a. The performance of the devices was optimized by screening the D/A ratios as well as solvent additives, such as chloronaphthalene (CN) and DIO (Tables S2-4). In the optimization process, 0.75% CN was used, while chloroform was used as the main solvent, PM6 concentration was 7 mg mL^{-1} with the D/A ratio of 1:1.2 (w/w). According to Figure 2b, the current density-voltage (*J-V*) curves of the corresponding optimized OSCs are depicted, and Table 1 provides the mean values of optimal photovoltaic parameters obtained from at least 10 devices.

Table 1. The optimal photovoltaic parameters of DTCBT-F0, DTCBT-F5 and DTCBT-F9-based OCSs.

Active layer	V_{OC} (V) [a]	J_{SC} (mA cm^{-2})	J_{cal} (mA cm^{-2}) [b]	FF (%)	PCE (%)
PM6:DTCBT-F0	0.932 [0.932±0.004]	19.1 [18.6±0.6]	18.8	63.9 [63.4±0.5]	11.4 [11.0±0.3]
PM6:DTCBT-F5	0.913 [0.913±0.003]	21.6 [21.1±0.7]	20.6	64.2 [63.7±0.6]	12.7 [12.3±0.4]
PM6:DTCBT-F9	0.908 [0.908±0.004]	21.0 [20.5±0.6]	20.3	60.8 [60.2±0.6]	11.6 [11.2±0.4]

[a] The statistical results were obtained from 10 devices. [b] J_{cal} values were obtained from the corresponding EQE curves.

The PM6:DTCBT-F5-based devices exhibit the best PCE of 12.7%, with J_{SC} as high as 21.6 mA cm^{-2} and the optimum FF of 64.2%. For reference, the nonfluorinated DTCBT-F0-based devices fabricated using the same conditions showed a PCE of 11.4% with an open circuit voltage (V_{OC}) of 0.932 V, a J_{SC} of 19.1 mA cm^{-2}, and an FF of 63.9%. While the devices based on multi-fluorinated DTCBT-F9 exhibited a PCE of 11.6%, with a J_{SC} of 21.0 mA cm^{-2}, and an FF of 60.8%. In the DTCBT-F5-based devices, the increased PCE can be primarily due to the significant enhancement in J_{SC} and FF values as observed, which could be a result of the favorable exciton dissociation and enhanced

charge transportation of the DTCBT-F5, combined with its excellent molecular stacking properties in the blend films. Figure 2c shows the external quantum efficiency (EQE) spectra, demonstrating nearly identical response edges, which is consistent with the film absorption result. It was determined that the integrated current J_{cal} of the DTCBT-F0, DTCBT-F5, and DTCBT-F9-based solar cells were 20.4, 20.6, and 20.3 mA cm^{-2}, respectively. EQE values exceeding 60% were obtained with the corresponding devices between 450 and 800 nanometers, where the highest value of DTCBT-F5 reached about 80%, demonstrating the efficient charge generation and transport within the device. The fact that DTCBT-F5 displayed a higher EQE response within the range of 450 nm to 600 nm was likely caused by its stronger aggregation characteristics, which facilitate molecular packing, thus demonstrating the feasibility of the fluorination strategy to enhance photovoltaic efficiency.

2.4. Charge Carrier Mobilities and Recombination Dynamics. To determine the impact of fluorination in the side chains on the charge recombination mechanism, we measured the relationship between J_{SC} and V_{OC} values of devices based on DTCBT-F0, DTCBT-F5, and DTCBT-F9 with varying light intensities (P_{light}). As shown in the Figure 2d, J_{SC} and P_{light} are related by $J_{SC} \propto P^{\alpha}$, where recombination is represented by the exponent factor α. When α approaches 1, it is apparent that the bimolecular recombination does not have to be considered, allowing effective transport of the free charge carriers.[51-52] The α value of the device based on DTCBT-F5 is 0.943, which is closer to 1 compared to devices based on DTCBT-F0 (0.939) and DTCBT-F9 (0.937). Therefore, introducing a suitable amount of fluorine atoms in the side chain of SMAs may effectively minimize the occurrence of bimolecular recombination in the corresponding device. According to the correlations between V_{OC} and P_{light} of devices based on DTCBT-F0, DTCBT-F5, and DTCBT-F9 in Figure 2e, $V_{OC} \propto nkT/q \ln(P_{\mathrm{light}})$, the slope factors ($n$) of the corresponding device is 1.98, 1.95, and 2.03, respectively. In comparison with other devices, the larger slope for the DTCBT-F9-based devices suggesting that the trap-assisted recombination within the devices is

dominant, consistent with the lower FF values observed in the device data.[53] As a result, the suitable slope factor of DTCBT-F5-based devices means that appropriate side-chain fluorination can effectively reduce charge recombination, promote effective dissociation of excitons in the active layer. We further performed the transient photocurrent (TPC) and the transient photovoltage (TPV) experiment (Figure S5) for these acceptors to investigate the charge extraction and recombination process. TPC experiments show that the charge sweep-out time of DTCBT-F0, DTCBT-F5, and DTCBT-F9-based solar cells are 1.08, 0.86, and 0.366 μs, respectively. The faster charge sweep-out within DTCBT-F5-based device indicating its larger charge extraction capability. Besides, the longer carrier lifetime observed in DTCBT-F5-based device suggest the less bimolecular recombination, which is in line with the results of recombination observed from light intensity measurement.

Then, the charge transport behavior of the OSCs based on DTCBT-F0, DTCBT-F5, and DTCBT-F9 was characterized using the space-charge-limited current (SCLC) method. The corresponding hole mobility (μ_h) values and the electron mobility (μ_e) values of the DTCBT-F0, DTCBT-F5, and DTCBT-F9-based blend films were shown in Figure S6 and Table S4, and the μ_h/μ_e was 1.48, 1.40, and 1.60, respectively. The charge carrier mobilities of the devices based on DTCBT-F5 are higher and are more balanced, compared to the nonfluorinated DTCBT-F0-based device, resulting in more favorable J_{SC} and FF values of the device. Meanwhile, DTCBT-F9 showed lower mobilities of charge carriers with increased fluorine content, possibly due to its stronger recombination, which resulted in a decreased device performance, further emphasizing the significance of appropriate side-chain fluorination in the charge transport process of non-fullerene SMA-based devices.

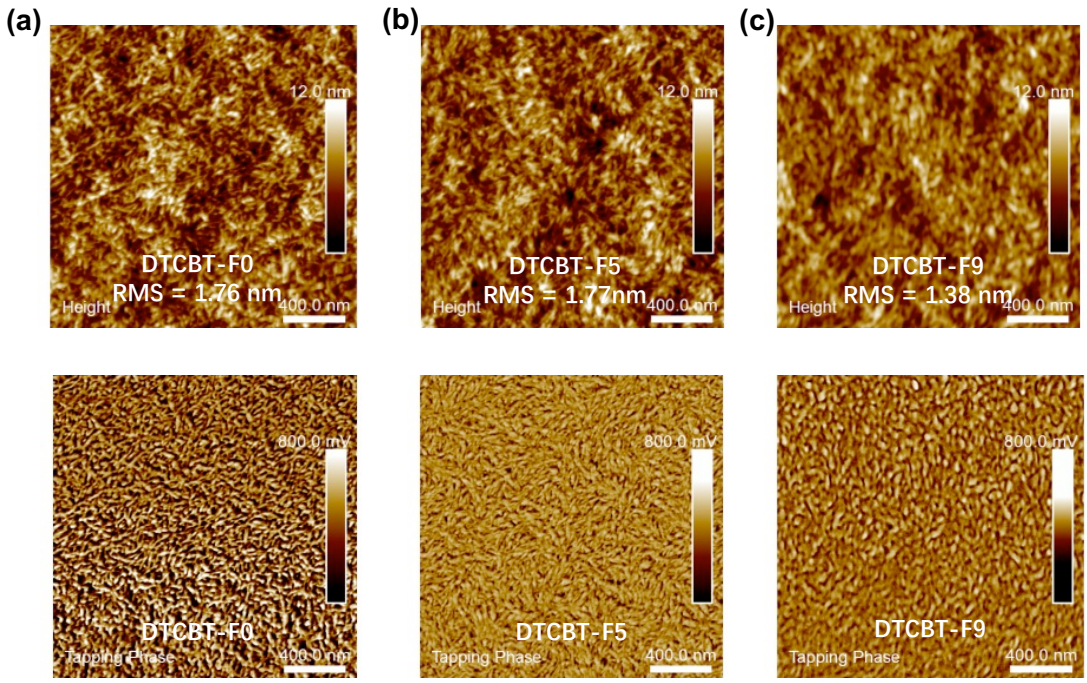

Figure 3. The AFM height (Top) and phase (Bottom) images for (a) DTCBT-F0, (b) DTCBT-F5, and (c) DTCBT-F9-based blend films.

2.5. Molecular Ordering and Blend Morphology. To further evaluate the influence of fluorine atoms to the surface morphologies, atomic force microscopy (AFM) measurements were conducted (Figure 3). It has been demonstrated that the corresponding root-mean-square (RMS) roughness values for the blend films based on DTCBT-F0, DTCBT-F5, and DTCBT-F9 were 1.76 nm, 1.77 nm, and 1.38 nm, respectively, which means that the DTCBT-F5-based blend film exhibits a rougher surface compared to the nonfluorinated blend film. It may be attributed to the stronger aggregation properties and higher crystallinity of DTCBT-F5, which makes the charge transport and collection in DTCBT-F5-based devices more efficient. Meanwhile, it can be observed that the surface morphologies of the blend film based on PM6:DTCBT-F5 have a uniform interpenetrating network structure, which could be attributed to the relatively matched surface energy between PM6 and DTCBT-F5, facilitating the desirable exciton dissociation and charge transfer in the device. Conversely, with an increasing fluorine content, DTCBT-F9 may be detrimental to the efficient dissociation of excitons at the D-A interface due to the low miscibility with PM6, resulting in a

decrease in PCE observed in DTCBT-F9-based devices.

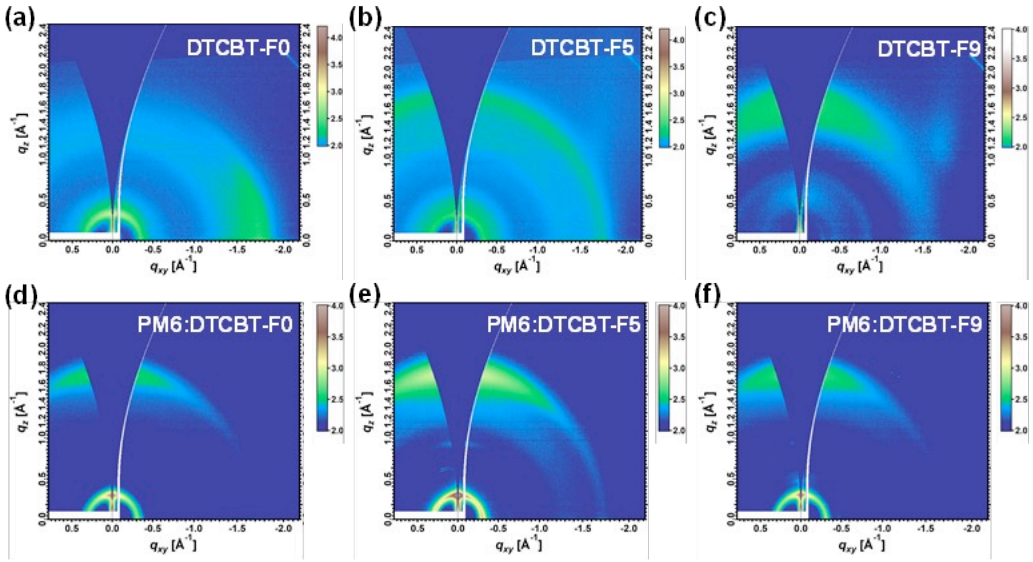

Figure 4. 2D-GIWAXS patterns of (a) DTCBT-F0, (b) DTCBT-F5, (c) DTCBT-F9, (d) PM6:DTCBT-F0, (e) PM6:DTCBT-F5 and (f) PM6:DTCBT-F9-based thin films.

The DTCBT-F0, DTCBT-F5, and DTCBT-F9 pure films and their corresponding blend films were subjected to grazing incident wide-angle X-ray scattering (GIWAXS) analysis to explore the influence of fluorination on molecular packing behavior and crystallinity. According to Figure 4, the 2D-GIWAXS patterns show that the introduction of fluorine atoms in the pure film results in a clear difference in molecular packing behavior. Different from the preferential edge-on orientation of the DTCBT-F0 pure film, with the introduction of fluorine atoms, the DTCBT-F5 pure film is characterized by a ring-like scattering feature, which are indicative of its mixed orientation. With increasing degrees of side chain fluorination, the (010) diffraction peaks displayed on the q_z axis of the DTCBT-F9 pure film indicate that its molecular packing is preferentially face-on direction. In addition, these blend films are also preferentially stacked in a face-on stacking orientation relative to the substrate, suggesting their different intermolecular interactions with the donor polymer. The π-π stacking distances (d_{010}) and corresponding (010) coherence lengths (CLs)[54] of DTCBT-F0, DTCBT-F5, and DTCBT-F9-based blend films derived from 1D profiles (Figure S7) are presented in Table S5. The calculated π-π CL according to Scherrer

analysis for polymer donor and non-fused SMA are found to be 33.56 and 38.47 Å for PM6:DTCBT-F5-based blend films, which are much higher than that of 27.86/33.68 and 20.94/29.76 Å for PM6:DTCBT-F0 and PM6:DTCBT-F9-based blend films, respectively. The increased CLs in the PM6:DTCBT-F5 blend indicates a stronger crystallinity of DTCBT-F5 in the blend film, while the greater stacking properties of PM6 correspond to enhanced EQE values mentioned above. It can be concluded that the tight packing in the vertical direction and excellent crystallinity of the DTCBT-F5-based blend film increase the efficiency of charge transfer within the device, which explains its higher J_{SC} mentioned above.

To understand the miscibility properties and phase separation morphology of three blend films, the contact angles of DTCBT-F0, DTCBT-F5, and DTCBT-F9 neat films were quantified employing deionized water and ethylene glycol as shown in Figure S8. The surface free energy (γ) was calculated by the following equation, $\gamma_s = \gamma_s^d + \gamma_s^p$. By estimating Flory-Huggins interaction parameters (χ), $\chi_{D-A} = \mathrm{K}(\sqrt{\gamma_D} - \sqrt{\gamma_A})^2$, the miscibility between the polymer donor and DTCBT-F0, DTCBT-F5, and DTCBT-F9 was explored. According to the data in Table S6, the contact angle increases with the introduction of fluorine atoms. The γ values of DTCBT-F9 (16.14 mJ m^{-2}) and DTCBT-F5 (17.86 mJ m^{-2}) are lower than that of the reference compound, DTCBT-F0 (17.93 mJ m^{-2}). Additionally, the χ values for DTCBT-F0, DTCBT-F5, and DTCBT-F9 are 0.38K, 0.39K, and 0.69K, respectively. It can be concluded that as fluorine content in the side chains increases, the corresponding γ value gradually decreases and the surface energy gap between PM6 and SMAs increases, which may favor the good vertical phase separation and suitable miscibility of DTCBT-F5 in the blend.[44] As a result of the large difference in γ between multi-fluorinated DTCBT-F9 and PM6, exciton dissociation and transfer may be adversely affected at the D-A interface within the active layer. The moderate surface parameters of DTCBT-F5 prove that it possesses suitable miscibility and good phase separation within the active layer, which can further explain its higher J_{SC} and PCE.

3. Conclusion

In conclusion, we have designed and synthesized three asymmetric non-fused SMAs based on fluorination strategy, and evaluate the effects of the number of fluorine atoms in side chains on the molecular packing and the corresponding device performance. The results exhibited that the light absorption, energy levels, as well as the molecular packing behavior and film morphology can be effectively modulated through side chain fluorination. DTCBT-F5-based blend film shows appropriate miscibility, diminished charge recombination and optimized charge carrier mobility. The PM6:DTCBT-F5-based devices obtained the best PCE of 12.7% with the highest J_{SC} of 21.6 mA cm^{-2} and the optimal FF of 64.2%, which outperform those devices based on DTCBT-F0 (11.4%) and DTCBT-F9 (11.6%), respectively. This work demonstrates that precise control of the fluorine functionalization in side chains of non-fused SMAs is an effective strategy to realizing high J_{SC} and FF towards highly efficient non-fused electron acceptor based OSCs.

4. Experimental section

4.1. Materials and Synthesis. Compounds 3, 4, and 8 were synthesized according to previous reports.[48] The synthesis details were provided in the supporting information. All reactions and manipulations were conducted under a nitrogen atmosphere using standard Schlenk techniques.

4.2 Device Fabrication and Characterization. The ITO-coated glass was cleaned inside an ultrasonic bath by using deionized water, acetone, and isopropyl alcohol sequentially. Prior to usage, the glass substrates underwent treatment with a UV−ozone cleaner for 20 minutes. A thin layer of PEDOT:PSS was spin-coated onto the ITO substrates at 4000 rpm for 30 seconds and then annealed at 150°C for 15 minutes. Following this, the PEDOT/PSS-coated ITO substrates were transferred to a glovebox. Then, the blend solution was spin-cast onto the PEDOT:PSS layer at 3000 rpm for 40 seconds. Subsequently, the samples were annealed at 100°C for 10 minutes. A thin layer of PNDIT-F3N was then coated, followed by the deposition of a 100 nm thick Ag layer. Photocurrent measurements were conducted under AM 1.5G (100 mW/cm^2) illumination using the Enlitech SSX50 solar simulator.

Supporting Information

The data that support the findings of this study are available in the supplementary material of this paper. Experimental details, instruments, device fabrication and characterization, NMR spectra, CV, MALDI-TOF MS spectra, DFT, UV−vis spectroscopy, SCLC, GIWAXS, and contact angle data.

Acknowledgements

The work described in this paper was supported by the National Natural Science Foundation of China (No. 52103202), the Fundamental Research Funds for the Central Universities (2232023A-01), the Key Lab of Fluorine and Silicon for Energy Materials and Chemistry of Ministry of Education, Jiangxi Normal University (No. KFSEMC-202202), and Shanxi-Zheda Institute of Advanced Materials and Chemical Engineering.

Conflict of interest

The authors declare no conflict of interest.

References

1. Zhang, G.; Zhao, J.; Chow, P. C. Y.; Jiang, K.; Zhang, J.; Zhu, Z.; Zhang, J.; Huang, F.; Yan, H., Nonfullerene Acceptor Molecules for Bulk Heterojunction Organic Solar Cells. *Chem. Rev.* **2018,** *118*, 3447-3507.

2. Li, Y.; Guo, X.; Peng, Z.; Qu, B.; Yan, H.; Ade, H.; Zhang, M.; Forrest, S. R., Color-neutral, semitransparent organic photovoltaics for power window applications. *Proc. Natl. Acad. Sci. U.S.A.* **2020,** *117*, 21147-21154.

3. Wang, G.; Zhang, J.; Yang, C.; Wang, Y.; Xing, Y.; Adil, M. A.; Yang, Y.; Tian, L.; Su, M.; Shang, W.; Lu, K.; Shuai, Z.; Wei, Z., Synergistic Optimization Enables Large-Area Flexible Organic Solar Cells to Maintain over 98% PCE of the Small-Area Rigid Devices. *Adv Mater* **2020,** *32*, 2005153.

4. Zhang, G.; Lin, F. R.; Qi, F.; Heumuller, T.; Distler, A.; Egelhaaf, H. J.; Li, N.; Chow, P. C. Y.; Brabec, C. J.; Jen, A. K.; Yip, H. L., Renewed Prospects for Organic Photovoltaics. *Chem Rev* **2022,** *122*, 14180-14274.

5. Liu, Y.; Liu, B.; Ma, C.-Q.; Huang, F.; Feng, G.; Chen, H.; Hou, J.; Yan, L.; Wei,

Q.; Luo, Q.; Bao, Q.; Ma, W.; Liu, W.; Li, W.; Wan, X.; Hu, X.; Han, Y.; Li, Y.; Zhou, Y.; Zou, Y.; Chen, Y.; Li, Y.; Chen, Y.; Tang, Z.; Hu, Z.; Zhang, Z.-G.; Bo, Z., Recent progress in organic solar cells (Part I material science). *Sci. China Chem.* **2021,** *65*, 224-268.

6. Yan, C.; Barlow, S.; Wang, Z.; Yan, H.; Jen, A. K. Y.; Marder, S. R.; Zhan, X., Non-fullerene acceptors for organic solar cells. *Nat. Rev. Mater.* **2018,** *3*, 18003.

7. Zhang, J.; Tan, H. S.; Guo, X.; Facchetti, A.; Yan, H., Material insights and challenges for non-fullerene organic solar cells based on small molecular acceptors. *Nat. Energy* **2018,** *3*, 720-731.

8. Yu, H.; Wang, Y.; Kim, H. K.; Wu, X.; Li, Y.; Yao, Z.; Pan, M.; Zou, X.; Zhang, J.; Chen, S.; Zhao, D.; Huang, F.; Lu, X.; Zhu, Z.; Yan, H., A Vinylene-Linker-Based Polymer Acceptor Featuring a Coplanar and Rigid Molecular Conformation Enables High-Performance All-Polymer Solar Cells with Over 17% Efficiency. *Adv Mater* **2022,** *34*, 2200361.

9. Chong, K.; Xu, X.; Meng, H.; Xue, J.; Yu, L.; Ma, W.; Peng, Q., Realizing 19.05% Efficiency Polymer Solar Cells by Progressively Improving Charge Extraction and Suppressing Charge Recombination. *Adv Mater* **2022,** *34*, 2109516.

10. Zhu, L.; Zhang, M.; Xu, J.; Li, C.; Yan, J.; Zhou, G.; Zhong, W.; Hao, T.; Song, J.; Xue, X.; Zhou, Z.; Zeng, R.; Zhu, H.; Chen, C.-C.; MacKenzie, R. C. I.; Zou, Y.; Nelson, J.; Zhang, Y.; Sun, Y.; Liu, F., Single-junction organic solar cells with over 19% efficiency enabled by a refined double-fibril network morphology. *Nat. Mater.* **2022,** *21*, 656-663.

11. Jiang, K.; Zhang, J.; Zhong, C.; Lin, F. R.; Qi, F.; Li, Q.; Peng, Z.; Kaminsky, W.; Jang, S.-H.; Yu, J.; Deng, X.; Hu, H.; Shen, D.; Gao, F.; Ade, H.; Xiao, M.; Zhang, C.; Jen, A. K. Y., Suppressed recombination loss in organic photovoltaics adopting a planar–mixed heterojunction architecture. *Nat. Energy* **2022,** *7*, 1076–1086.

12. Zheng, Z.; Wang, J.; Bi, P.; Ren, J.; Wang, Y.; Yang, Y.; Liu, X.; Zhang, S.; Hou, J., Tandem Organic Solar Cell with 20.2% Efficiency. *Joule* **2022,** *6*, 171-184.

13. Zhao, C.; Ma, R.; Hou, Y.; Zhu, L.; Zou, X.; Xiong, W.; Hu, H.; Wang, L.; Yu, H.; Wang, Y.; Zhang, G.; Yi, J.; Chen, L.; Wu, D.; Yang, T.; Li, G.; Qiu, M.; Yan, H.; Li, S.;

Zhang, G., 18.1% Ternary All-Polymer Solar Cells Sequentially Processed from Hydrocarbon Solvent with Enhanced Stability. *Adv. Energy Mater.* **2023,** *13*, 2300904.

14. Yuan, J.; Zhang, Y.; Zhou, L.; Zhang, G.; Yip, H.-L.; Lau, T.-K.; Lu, X.; Zhu, C.; Peng, H.; Johnson, P. A.; Leclerc, M.; Cao, Y.; Ulanski, J.; Li, Y.; Zou, Y., Single-Junction Organic Solar Cell with over 15% Efficiency Using Fused-Ring Acceptor with Electron-Deficient Core. *Joule* **2019,** *3*, 1140-1151.

15. Lin, Y.; Wang, J.; Zhang, Z. G.; Bai, H.; Li, Y.; Zhu, D.; Zhan, X., An Electron Acceptor Challenging Fullerenes for Efficient Polymer Solar Cells. *Adv. Mater.* **2015,** *27*, 1170-1174.

16. Zhou, Y.; Li, M.; Lu, H.; Jin, H.; Wang, X.; Zhang, Y.; Shen, S.; Ma, Z.; Song, J.; Bo, Z., High-Efficiency Organic Solar Cells Based on a Low-Cost Fully Non-Fused Electron Acceptor. *Adv. Funct. Mater.* **2021,** *31*, 2101742.

17. Li, C.; Zhang, X.; Yu, N.; Gu, X.; Qin, L.; Wei, Y.; Liu, X.; Zhang, J.; Wei, Z.; Tang, Z.; Shi, Q.; Huang, H., Simple Nonfused-Ring Electron Acceptors with Noncovalently Conformational Locks for Low-Cost and High-Performance Organic Solar Cells Enabled by End-Group Engineering. *Adv. Funct. Mater.* **2021,** *32*, 2108861.

18. Li, S.; Zhan, L.; Liu, F.; Ren, J.; Shi, M.; Li, C. Z.; Russell, T. P.; Chen, H., An Unfused-Core-Based Nonfullerene Acceptor Enables High-Efficiency Organic Solar Cells with Excellent Morphological Stability at High Temperatures. *Adv Mater* **2018,** *30*, 1705208.

19. Ma, L.; Zhang, S.; Zhu, J.; Wang, J.; Ren, J.; Zhang, J.; Hou, J., Completely non-fused electron acceptor with 3D-interpenetrated crystalline structure enables efficient and stable organic solar cell. *Nat. Commun.* **2021,** *12*, 5093.

20. Huang, H.; Guo, Q.; Feng, S.; Zhang, C.; Bi, Z.; Xue, W.; Yang, J.; Song, J.; Li, C.; Xu, X.; Tang, Z.; Ma, W.; Bo, Z., Noncovalently fused-ring electron acceptors with near-infrared absorption for high-performance organic solar cells. *Nat. Commun.* **2019,** *10*, 3038.

21. Ye, L.; Hu, H.; Ghasemi, M.; Wang, T.; Collins, B. A.; Kim, J. H.; Jiang, K.; Carpenter, J. H.; Li, H.; Li, Z.; McAfee, T.; Zhao, J.; Chen, X.; Lai, J. L. Y.; Ma, T.; Bredas, J. L.; Yan, H.; Ade, H., Quantitative relations between interaction parameter,

miscibility and function in organic solar cells. *Nat. Mater.* **2018,** *17*, 253-260.

22. Zhang, J.; Luo, S.; Zhao, H.; Xu, X.; Zou, X.; Shang, A.; Liang, J.; Bai, F.; Chen, Y.; Wong, K. S.; Ma, Z.; Ma, W.; Hu, H.; Chen, Y.; Yan, H., Precise Control of Selenium Functionalization in Non-Fullerene Acceptors Enabling High-Efficiency Organic Solar Cells. *Angew. Chem. Int. Ed. Engl.* **2022,** *61*, e202206930.

23. Weng, K.; Ye, L.; Zhu, L.; Xu, J.; Zhou, J.; Feng, X.; Lu, G.; Tan, S.; Liu, F.; Sun, Y., Optimized active layer morphology toward efficient and polymer batch insensitive organic solar cells. *Nat. Commun.* **2020,** *11*, 2855.

24. Fan, B.; Lin, F.; Wu, X.; Zhu, Z.; Jen, A. K., Selenium-Containing Organic Photovoltaic Materials. *Acc. Chem. Res.* **2021,** *54*, 3906-3916.

25. Dai, S.; Xiao, Y.; Xue, P.; James Rech, J.; Liu, K.; Li, Z.; Lu, X.; You, W.; Zhan, X., Effect of Core Size on Performance of Fused-Ring Electron Acceptors. *Chem. Mater.* **2018,** *30*, 5390-5396.

26. Li, T.; Dai, S.; Ke, Z.; Yang, L.; Wang, J.; Yan, C.; Ma, W.; Zhan, X., Fused Tris(thienothiophene)-Based Electron Acceptor with Strong Near-Infrared Absorption for High-Performance As-Cast Solar Cells. *Adv. Mater.* **2018,** *30*, 1705969.

27. Zhao, W.; Li, S.; Yao, H.; Zhang, S.; Zhang, Y.; Yang, B.; Hou, J., Molecular Optimization Enables over 13% Efficiency in Organic Solar Cells. *J. Am. Chem. Soc.* **2017,** *139*, 7148-7151.

28. Zhang, J.; Li, Y.; Hu, H.; Zhang, G.; Ade, H.; Yan, H., Chlorinated Thiophene End Groups for Highly Crystalline Alkylated Non-Fullerene Acceptors toward Efficient Organic Solar Cells. *Chem. Mater.* **2019,** *31*, 6672-6676.

29. Zhao, Q.; Qu, J.; He, F., Chlorination: An Effective Strategy for High-Performance Organic Solar Cells. *Adv. Sci.* **2020,** *7*, 2000509.

30. Li, S.; Ye, L.; Zhao, W.; Zhang, S.; Ade, H.; Hou, J., Significant Influence of the Methoxyl Substitution Position on Optoelectronic Properties and Molecular Packing of Small-Molecule Electron Acceptors for Photovoltaic Cells. *Adv. Energy Mater.* **2017,** *7*, 1700183.

31. Li, S.; Ye, L.; Zhao, W.; Zhang, S.; Mukherjee, S.; Ade, H.; Hou, J., Energy-Level Modulation of Small-Molecule Electron Acceptors to Achieve over 12% Efficiency in

Polymer Solar Cells. *Adv Mater* **2016,** *28*, 9423-9429.

32. Zhang, X.; Qin, L.; Yu, J.; Li, Y.; Wei, Y.; Liu, X.; Lu, X.; Gao, F.; Huang, H., High-performance Unfused-Ring Electron Acceptors for Organic Solar Cells Enabled by Noncovalent Intramolecular Interactions and End Group Engineering. *Angew. Chem. Int. Ed. Engl.* **2021,** *22*, 12583-12589.

33. Shang, A.; Luo, S.; Zhang, J.; Zhao, H.; Xia, X.; Pan, M.; Li, C.; Chen, Y.; Yi, J.; Lu, X.; Ma, W.; Yan, H.; Hu, H., Over 18% Binary Organic Solar Cells Enabled by Isomerization of Non-Fullerene Acceptors with Alkylthiophene Side Chains. *Sci. China Chem.* **2022,** *65*, 1758.

34. Deng, M.; Xu, X.; Duan, Y.; Yu, L.; Li, R.; Peng, Q., Y-Type Non-Fullerene Acceptors with Outer Branched Side Chains and Inner Cyclohexane Side Chains for 19.36% Efficiency Polymer Solar Cells. *Adv Mater* **2023,** *35*, 2210760.

35. Chen, Y.; Meng, H.; Ding, L.; Tang, J.; Yi, J.; Zhang, J.; Wang, Z.; Ma, R.; Li, Z.; Lyu, L.; Xu, X.; Li, R.; Peng, Q.; Yan, H.; Hu, H., Asymmetric Non-Fullerene Acceptors with Branched Alkyl-Chains for Efficient Organic Solar Cells with High Open-Circuit Voltage. *Chem. Mater.* **2022,** *34*, 10144-10152.

36. Chen, Y.; Chang, Y.; Ma, R.; Liu, H.; Yi, J.; Zhang, J.; Liu, T.; Qi, Z.; Yu, K.; Lu, X.; Hu, H.; Yan, H., Side-chain engineering with chalcogen-containing heterocycles on non-fullerene acceptors for efficient organic solar cells. *Chem. Eng. J.* **2022,** *441*, 135998.

37. Hai, J.; Song, Y.; Li, L.; Liu, X.; Shi, X.; Huang, Z.; Qian, G.; Lu, Z.; Yu, J.; Hu, H.; Chen, S., High-Efficiency Organic Solar Cells Enabled by Chalcogen Containing Branched Chain Engineering: Balancing Short-Circuit Current and Open-Circuit Voltage, Enhancing Fill Factor. *Adv. Funct. Mater.* **2023,** *33*, 2213429.

38. Zhang, Q.; Kelly, M. A.; Bauer, N.; You, W., The Curious Case of Fluorination of Conjugated Polymers for Solar Cells. *Acc. Chem. Res.* **2017,** *50*, 2401-2409.

39. Yu, H.; Wang, Y.; Zou, X.; Han, H.; Kim, H. K.; Yao, Z.; Wang, Z.; Li, Y.; Ng, H. M.; Zhou, W.; Zhang, J.; Chen, S.; Lu, X.; Wong, K. S.; Zhu, Z.; Yan, H.; Hu, H., Effects of Halogenation of Small-molecule and Polymeric Acceptors for Efficient Organic Solar Cells. *Adv. Funct. Mater.* **2023,** *33*, 2300712.

40. Wang, M.; Ford, M. J.; Zhou, C.; Seifrid, M.; Nguyen, T. Q.; Bazan, G. C., Linear Conjugated Polymer Backbones Improve Alignment in Nanogroove-Assisted Organic Field-Effect Transistors. *J. Am. Chem. Soc.* **2017,** *139*, 17624-17631.

41. Yu, H.; Pan, M.; Sun, R.; Agunawela, I.; Zhang, J.; Li, Y.; Qi, Z.; Han, H.; Zou, X.; Zhou, W.; Chen, S.; Lai, J. Y. L.; Luo, S.; Luo, Z.; Zhao, D.; Lu, X.; Ade, H.; Huang, F.; Min, J.; Yan, H., Regio-Regular Polymer Acceptors Enabled by Determined Fluorination on End Groups for All-Polymer Solar Cells with 15.2% Efficiency. *Angew. Chem. Int. Ed. Engl.* **2021,** *60*, 10137.

42. Lai, H.; Zhao, Q.; Chen, Z.; Chen, H.; Chao, P.; Zhu, Y.; Lang, Y.; Zhen, N.; Mo, D.; Zhang, Y.; He, F., Trifluoromethylation Enables a 3D Interpenetrated Low-Band-Gap Acceptor for Efficient Organic Solar Cells. *Joule* **2020,** *4*, 688-700.

43. Yao, C.; Zhao, J.; Zhu, Y.; Liu, B.; Yan, C.; Perepichka, D. F.; Meng, H., Trifluoromethyl Group-Modified Non-Fullerene Acceptor toward Improved Power Conversion Efficiency over 13% in Polymer Solar Cells. *ACS. Appl. Mater. Interfaces* **2020,** *12*, 11543-11550.

44. Chen, S.; Hong, L.; Dong, M.; Deng, W.; Shao, L.; Bai, Y.; Zhang, K.; Liu, C.; Wu, H.; Huang, F., A Polyfluoroalkyl-Containing Non-fullerene Acceptor Enables Self-Stratification in Organic Solar Cells. *Angew. Chem. Int. Ed. Engl.* **2023,** *62*, e202213869.

45. Hou, R.; Li, M.; Ma, X.; Huang, H.; Lu, H.; Jia, Q.; Liu, Y.; Xu, X.; Li, H. B.; Bo, Z., Noncovalently Fused-Ring Electron Acceptors with C2v Symmetry for Regulating the Morphology of Organic Solar Cells. *ACS Appl. Mater. Interfaces* **2020,** *12*, 46220-46230.

46. Yu, K.; Pan, M.; Xu, X.; Zhang, J.; Wang, Z.; Cui, Y.; Huang, Y.; Liao, Y.; Yan, H.; Hu, H., Isomerization of Noncovalently Conformational Lock in Nonfused Electron Acceptor toward Efficient Organic Solar Cells. *ACS Appl. Energy Mater.* **2022,** *5*, 10224-10232.

47. Wang, X.; Lu, H.; Zhang, A.; Yu, N.; Ran, G.; Bi, Z.; Yu, X.; Xu, X.; Liu, Y.; Tang, Z.; Zhang, W.; Ma, W.; Bo, Z., Molecular-Shape-Controlled Nonfused Ring Electron Acceptors for High-Performance Organic Solar Cells with Tunable Phase Morphology.

ACS Appl. Mater. Interfaces **2022,** *14*, 28807-28815.

48. Wen, T. J.; Liu, Z. X.; Chen, Z.; Zhou, J.; Shen, Z.; Xiao, Y.; Lu, X.; Xie, Z.; Zhu, H.; Li, C. Z.; Chen, H., Simple Non-Fused Electron Acceptors Leading to Efficient Organic Photovoltaics. *Angew. Chem. Int. Ed. Engl.* **2021,** *22*, 12964-12970.

49. Pang, S.; Mas-Montoya, M.; Xiao, M.; Duan, C.; Wang, Z.; Liu, X.; Janssen, R. A. J.; Yu, G.; Huang, F.; Cao, Y., Adjusting Aggregation Modes and Photophysical and Photovoltaic Properties of Diketopyrrolopyrrole-Based Small Molecules by Introducing B<--N Bonds. *Chem. Eur. J* **2019,** *25*, 564-572.

50. Bredas, J.-L., Mind the gap! *Mater. Horiz.* **2014,** *1*, 17-19.

51. Cowan, S. R.; Roy, A.; Heeger, A. J., Recombination in polymer-fullerene bulk heterojunction solar cells. *Phys. Rev. B* **2010,** *82*, 245207.

52. Koster, L. J. A.; Mihailetchi, V. D.; Xie, H.; Blom, P. W. M., Origin of the light intensity dependence of the short-circuit current of polymer/fullerene solar cells. *Appl. Phys. Lett.* **2005,** *87*, 203502

53. Mandoc, M. M.; Kooistra, F. B.; Hummelen, J. C.; de Boer, B.; Blom, P. W. M., Effect of traps on the performance of bulk heterojunction organic solar cells. *Appl. Phys. Lett.* **2007,** *91*, 263505.

54. Smilgies, D. M., Scherrer grain-size analysis adapted to grazing-incidence scattering with area detectors. *J. Appl. Crystallogr.* **2009,** *42*, 1030-1034.

Table of Contents graphic

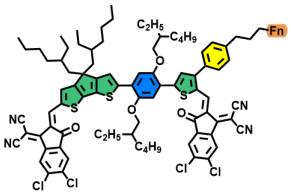

DTCBT-F0, Fn = C_2H_5
DTCBT-F5, Fn = C_2F_5
DTCBT-F9, Fn = C_4F_9